Level Set Method for Positron Emission Tomography

Marius Lysaker, Tony Chan and Xue-Cheng Tai

M. Lysaker and X-C. Tai are with the Department of Mathematics, University of Bergen, Johannes Brunsgate 12, N-5009 Bergen, Norway, Email: mariusl@mi.uib.no and tai@mi.uib.no. T. Chan is with the Department of Mathematics, University of California, Los Angeles, 405 Hilgard Avenue, Los Angeles, CA 90095-1555. USA, Email: TonyC@college.ucla.edu.

We acknowledge support from the NSF under contracts NSF ACI-0072112, NSF INT-0072863, NSF DMS 99-73341, from the ONR under grant N00014-96-1-10277, and from the NIH under grant P20MH65166, from the Norwegian Research Council of Norway and from CMA (Center of Mathematics for Applications) and from CIPR (Center for integrated Petroleum Research).

Abstract

In positron emission tomography (PET) a radioactive compound is injected into the body to promote a tissue dependent emission rate. Expectation Maximization (EM) reconstruction algorithms are iterative techniques which estimate the concentration coefficients that provides the best fitted solution, e.g. a maximum likelihood estimate. For some applications of PET, the aim is to identify the shape of the radioactive objects, and not only reveal the radioactive distribution. In this paper we propose a variant of the EM algorithm that generates successive adjustments to the shape of these objects to find the best fitted solution. This is an attractive approach for those applications of PET where the shape of special objects (e.g. tumors) should be identified. We utilize a multiple level set formulation to represent the geometry of the objects in the scene. The proposed algorithm can be applied to any PET configuration, without major modifications.

Keywords

Level set, PET, image processing, inverse problems, geometry.

I. Introduction

One of the most important quality of PET is its ability to model biological and physiological functions in vivo to enhance our understanding of the biochemical basis of normal and abnormal functions within the body. PET is also useful for the detection of cancer, coronary artery disease and brain disease. During a PET acquisition a compound containing a radiative isotope is injected into the body to form an (unknown) emission density $\lambda(x, y) \geq 0$. The positron emitted finds a nearby electron and annihilates into two photons of 511 keV according to the equation $E = mc^2$. This energy is strong enough to escape the body. Since the two photons travel at almost opposite directions, a detector ring surrounds the patient and collects all the emissions. For an emission event to be counted, both photons must be registered nearly simultaneously at two opposite detectors. In Fig. 1 emission paths from two different regions are shown, i.e. along the tube covered by detector pair AD, and along the tube covered by detector pair BC. Regions with higher concentration of radioactivity cause a higher emission rate. Given the total number of measured counts for each detector pair, the challenge is to locate all the emission sources inside the detector ring. Emissions measured between two detectors could have taken place anywhere along the tube between these two detectors, but with a systematic inspection

of all detector pairs, it is possible to reveal variance in the emission rate along the same tube.

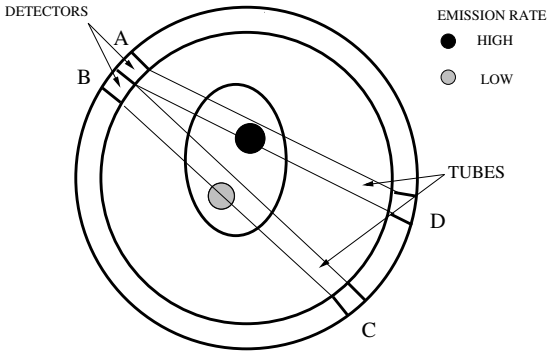

Fig. 1. Gamma-rays escape the body and are observed by the detectors.

Detection of the radioactive concentration in different tissues gives useful information both for research and clinical purposes. This information is often analyzed and visualized as an image. Unfortunately, the measured events also include noise such as accidental coincidences that complicate the image construction. The Fourier-based filtered back-projection [1] algorithm is a well established construction technique. This algorithm is computationally efficient but the drawbacks are constructions with low signal-to-noise-ratio and low resolution. Iterative methods to construct PET images have been an attractive approach during the last two decades. Most of these methods are based on maximum likelihood estimates. Due to the inherent ill-posedness of this inverse problem, the reconstructed images will have noise and edge artifacts, see [2], [3] for related problems. It is well known that the standard EM algorithm [4], [5], [6] converges toward a noisy image and it is necessary to terminate the iteration before the noise becomes too dominant [7]. If the iteration stops too early, important information could be lost. A general approach to address these problems is to utilize a regularization term according to certain a priori assumptions of the desired image [8], [9], [10]. Results with deviation from these assumptions will be penalized. For example, information from surrounding pixels can reveal irregularities and remove outsiders. The total variation (TV) minimization has successfully been used in many image processing applications [11], [12] among others. In [13] the standard EM algorithm for PET was modified to incorporate the TV regularization. The blurring

effect was subdued using this approach, but improvements are still needed.

Common for the iterative methods mention above is that they estimate the concentration coefficients that provides the best fitted solution based on a maximum likelihood estimate. For some applications of PET the aim is to identify the shape of the radioactive objects, and not only reveal the radioactive distribution. The novelty in this paper is to propose a variant of the EM algorithm that generates successive adjustments to the shape of these objects to find the best fitted solution. This is an attractive approach for those applications of PET where the shape of special objects (e.g. tumors) should be identified. In order to reconstruct better images, we reduce the set of possible solution by estimating the emission rate as a piecewise constant function. We assume the constant values are approximately known and try to locate the discontinuities of the piecewise constant function. A multiple level set formulation is used to represent the geometry of the objects in the scene. Level set method is a technique developed to handle topological changes in a moving front (i.e. region boundaries) [14], [15], [16], [17]. By incorporating the level set method into the image construction, sharp boundaries between different tissues are directly given for PET images. This variant of the EM algorithm can be applied to any PET configuration, without major modifications. In our work we may also derive advantages from side information (MR or SPECT) to improve the image construction capacity.

Geometric curve-evolution techniques for tomograpic reconstruction problems have been proposed before, see [18], [19], [20] and the references therein. Simmular to [18], we assume the object intensity values to be piecewise constant, but as in [19] we allow for multiple object regions. However, due to the piesewise constant intensity value restriction, our cost functinal is simpler than the one they propose in [19].

The remaining of this paper is organized in the following way. In Section II we summarize the theory behind the EM approach and introduce specific notations used throughout this paper. Partial differential equation techniques have successfully been used in many image processing applications, and a predecessor for our approach is given in Section III. In Section IV we explain the main idea behind the level set method and demonstrate that level set functions can be used to represent general piecewise constant functions [21]. Motivated by this we utilize a level set formulation to represent PET images with piecewise constant

emission densities in Section V. In this section we also give implementation details. Finally, in Section VI we report some numerical results.

II. Maximum likelihood expectation maximization

From the measured emission an image can be constructed by the EM algorithm [5], [6]. This algorithm provides an iterative formula to construct an image which makes the measured data most likely to occur. Given an image, the aim to maximize the conditional probability of the data by using a likelihood function (and later we will also use a log-likelihood function):

$$l(\lambda) = f(data|\lambda) \qquad \text{or} \qquad l_{log}(\lambda) = \log(l(\lambda)). \tag{1}$$

Here, data is the measured counts in the detector ring and $\lambda : \Omega \rightarrow \mathbb{R}$ is the unknown emission rate causing these counts, and Ω is the image domain. The region to be reconstructed is usually covered by a uniform mesh where each square in the mesh corresponds to one pixel in the PET image. The discrete representation of λ, and other essential notations for describing the EM image reconstruction model are listed in Table I.

b	pixel index $(1, 2, \ldots, B)$.
λ_b	unknown source intensity at a pixel b, $\lambda_b \geq 0$ $\forall b$.
t	detector pair index $(1, 2, \ldots, T)$.
n_t	total number of coincidences counted by detector pair t, $n_t \geq 0$ $\forall t$.
P_{tb}	probability for an emission from b to be detected in t.

TABLE I

Notations used throughout this paper.

Each element P_{tb} in matrix P describes the probability for an annihilation event that occurred in the area of the source covered by pixel b to be detected by detector pair t. Several physical factors such as attenuation, scatter and accidental coincidence corrections, time-of-flight, positron range and angulation information etc. can be incorporated in the probability matrix P. To compute P_{tb} the angle-of-view method was chosen in this paper, but other methods can also be used [22], [23]. By the angle-of-view method each element

P_{tb} in the probability matrix P is approximated by the largest angle (in fraction of π) completely contained within tube t as seen from the center of b. For details about the angle-of-view see the paper of Sheep and Vardi [6]. The intensity value λ_b is the information we search since it is related to the tracer concentration. During the acquisition process a random number of emission is generated from a Poisson distribution. A non-negative, integer-valued, random variable Z follows a Poisson distribution if

$$Poisson(Z = k) = e^{-\sigma}\frac{\sigma^k}{k!} \tag{2}$$

where $\sigma > 0$ and Z has mean E(Z)=σ. The Poisson distribution is applicable to many problems involving random events, such as particles leaving a fixed point at a random angle. For a moment we focus on one of the tubes in Fig. 1 and assume this tube corresponds to the region covered by detector pair $t = 1$. Given the mean $(P\lambda)_1$ we want to maximize the probability for $(P\lambda)_1$ to fit the measured data n_1:

$$\begin{aligned} Poisson(Z = n_1) =& e^{-(P\lambda)_1}\frac{(P\lambda)_1^{n_1}}{n_1!} \\ &\Downarrow \\ \frac{\partial}{\partial(P\lambda)_1}Poisson(Z = n_1) =& \frac{e^{-(P\lambda)_1}(P\lambda)_1^{n_1-1}}{n_1!}(n_1 - (P\lambda)_1) = 0, \end{aligned} \tag{3}$$

where a maximum is obtained for $n_1 = (P\lambda)_1$, and similarly the maximum is achieved for $n_2 = (P\lambda)_2$ if we focus on region covered by detector pair $t = 2$. The measured coincidence events also include scattered and accidental coincidences. Some events produced inside the source pass undetected because of tissue attenuation or photon traveling path that do not intersect the detector ring. This complicates the image construction. However, each n_t is distributed according to a Poisson distribution and since all measurements are independent of each other, the likelihood over all projections reduces to the product of the separate projections likelihood [5]. Therefore we want to maximize

$$l(\lambda) = \prod_{t=1}^{T} e^{-(P\lambda)_t}\frac{(P\lambda)_t^{n_t}}{n_t!}. \tag{4}$$

To simplify the calculation, the log-likelihood function is employed to convert (4) to the form

$$l_{log}(\lambda) = \sum_{t=1}^{T}[\log e^{-(P\lambda)_t} + \log(P\lambda)_t^{n_t} - \log(n_t!)] = -\sum_{b=1}^{B}\lambda_b + \sum_{t=1}^{T} n_t \log(P\lambda)_t + K. \tag{5}$$

In (5) we exploit the conversions

$$\sum_{t=1}^{T}(P\lambda)_t = \sum_{b=1}^{B}\lambda_b \quad \text{and} \quad -\sum_{t=1}^{T}\log(n_t!) = K.$$

Since K is independent of λ this constant will be ignored. Maximizing $l_{log}(\lambda)$ with respect to λ will provide us with the best estimate of λ in a statistical sense. The optimization problem can be rewritten by $\max l_{log}(\lambda) = \min -l_{log}(\lambda)$ and thereupon a mathematical formulation of PET becomes

$$\min_{\lambda} F(\lambda) = \min_{\lambda}\Big(\sum_{b=1}^{B}\lambda_b - \sum_{t=1}^{T} n_t \log\left(P\lambda\right)_t + V(\lambda)\Big), \tag{6}$$

where $V(\lambda)$ is a regularization term introduced to improve image quality [7], [8], [9], [10], [13], [24]. Several regularization methods tend to blur edges because both noise and edges contribute to inhomogeneous behavior. To subdue the blurring effect, the total variation norm of λ was introduced as a regularization term in [13]. In the next section we give a short overview of the TV-based EM algorithm. This algorithm is related to our approach and some of the calculations derived below are needed for our level set algorithm described in Section V.

III. A total variation based EM algorithm

In [13], an algorithm was designed to find the pointwise values of λ. The authors covered the domain Ω with a uniform mesh where each square in the mesh corresponds to one pixel in the PET image. The emission density function λ is represented by a piecewise linear function or piecewise constant function where λ takes value λ_b at pixel b, $b = 1, 2, \ldots, B$. In order to regularize the problem, they tried to find a minimizer for the following functional

$$L(\lambda) = \alpha\int_{\Omega}|\nabla\lambda|dx + \Big(\sum_{b=1}^{B}\lambda_b - \sum_{t=1}^{T} n_t \log\left(P\lambda\right)_t\Big). \tag{7}$$

Let $\vec{\lambda} = \{\lambda_b\}_{b=1}^{B}$ be the vector containing the values of λ at pixels $1, 2, \ldots, B$. With this notation, it is easy to calculate for (7) that

$$\frac{\partial L}{\partial \vec{\lambda}} = \alpha C(\vec{\lambda})\vec{\lambda} + \vec{e} - P^t(\vec{n}./P\vec{\lambda}). \tag{8}$$

In the above, $C(\vec{\lambda})$ is a matrix depending on $\vec{\lambda}$, $\vec{e}$ is the vector with unit entries, P^t is the transpose of the matrix P and $\vec{n}./P\vec{\lambda}$ is the element wise division of vector $\vec{n}$ by vector $P\vec{\lambda}$. If in (8) we assume a steady state solution and approximate $\vec{e}$ by $\vec{\lambda}^{k+1}./\vec{\lambda}^k$, the One-Step-Late (OSL) algorithm [13] is the following fixed point iteration for finding the minimizer of (7)

$$\vec{\lambda}^{k+1} = \left[\alpha C(\vec{\lambda}^k) + \mathrm{diag}(1./\vec{\lambda}^k)\right]^{-1} P^t(\vec{n}./P\vec{\lambda}^k). \tag{9}$$

In (9) $\mathrm{diag}(1./\vec{\lambda}^k)$ is the matrix with $1./\vec{\lambda}^k$ on its diagonal and $C(\vec{\lambda}^k)$ is a finite difference approximation for $-\nabla \cdot (\nabla\vec{\lambda}^k./|\nabla\vec{\lambda}^k|)$. This algorithm finds all the pixel values λ_b. In practice, we know that λ can only take a few constant values in PET images. However, this information is not used in the above algorithm. Below we demonstrate that such information can be incorporated and handled in an efficient way by using the level set framework. See also [25], [26] for other applications where level set based ideas are used to identify piecewise constant functions.

IV. An introduction to the level set method

The level set method was proposed in Osher and Sethian [14] for tracing interfaces between different phases of fluid flows. Later it has been used in many applications involving movement of interfaces for different kind of physical problems [15], [16], [17]. In the following we shall present a "unified" framework, first presented in [21], [27], of using multiple level sets to represent piecewise constant functions, and use this to identify the function λ.

Let Γ be a closed curve in $\Omega \subset I\!R^2$. Associated with Γ, we define a ϕ as the signed distance function:

$$\phi(x) = \begin{cases} \mathrm{distance}(x,\Gamma), & x \in \text{interior of } \Gamma \\ -\mathrm{distance}(x,\Gamma), & x \in \text{exterior of } \Gamma. \end{cases}$$

It is clear that Γ is the zero level set of the function ϕ. In the case where Γ is not closed, but divide the domain into two parts, the level set function can be defined to be positive on one side of the curve and negative on the other side of the curve.

Once the level set function is defined, we can use it to represent general piecewise constant functions. For example, assuming that $\lambda(x)$ equals c_1 inside Γ and equals c_2

outside Γ, we see that λ can be represented as

$$\lambda = c_1 H(\phi) + c_2 \left(1 - H(\phi)\right), \tag{10}$$

where the Heaviside function $H(\phi)$ is defined by

$$H(\phi) = \begin{cases} 1, & \phi > 0 \\ 0, & \phi \leq 0. \end{cases}$$

In order to identify the piecewise constant function λ, we need to identify the level set function ϕ and the coefficients c_i, $i = 1, 2$.

If the function $\lambda(x)$ has many pieces, we need to use multiple level set functions. We follow the ideas of Chan and Vese [21], [28]. Assume that we have two closed curves Γ_1 and Γ_2, and we associate the two level set functions ϕ_j, $j = 1, 2$ with these curves. The domain Ω can now be divided into four parts:

$$\begin{aligned} \Omega_1 &= \{x \in \Omega, \quad \phi_1 > 0, \quad \phi_2 > 0\}, \\ \Omega_2 &= \{x \in \Omega, \quad \phi_1 > 0, \quad \phi_2 < 0\}, \\ \Omega_3 &= \{x \in \Omega, \quad \phi_1 < 0, \quad \phi_2 > 0\}, \\ \Omega_4 &= \{x \in \Omega, \quad \phi_1 < 0, \quad \phi_2 < 0\}. \end{aligned} \tag{11}$$

Using the Heaviside function again, we can express λ with possibly up to four pieces of constant values:

$$\begin{aligned} \lambda = {} & c_1 H(\phi_1) H(\phi_2) + c_2 H(\phi_1)(1 - H(\phi_2)) \\ & + c_3 (1 - H(\phi_1)) H(\phi_2) + c_4 (1 - H(\phi_1))(1 - H(\phi_2)). \end{aligned} \tag{12}$$

By generalizing, we see that n level set functions give the possibility of 2^n regions. For $i = 1, 2, \ldots, 2^n$, let

$$\text{bin}(i-1) = (b_1^i, b_2^i, \ldots, b_n^i)$$

be the binary representation of $i - 1$, where $b_j^i = 0$ or 1. A piecewise constant function λ with constant coefficients c_i, $i = 1, 2, \ldots 2^n$ can be represented as (c.f. [26], [27])

$$\lambda = \sum_{i=1}^{2^n} c_i \prod_{j=1}^{n} R_i(\phi_j), \tag{13}$$

where

$$R_i(\phi_j) = \begin{cases} H(\phi_j), & \text{if } b_j^i = 0; \\ 1 - H(\phi_j), & \text{if } b_j^i = 1. \end{cases}$$

Even if the true λ needs less than 2^n distinct regions, we can still use n level set functions since some sub-domains are allowed to be empty. Using such a representation, we only need to determine the maximum number of level set functions that should be utilized.

For some applications, the function value inside each region may not be a constant and change slowly. Thus, we may try to use quadratic, cubic or some higher order polynomials to approximate the function inside each region. However, in this paper we focus on piecewise constant representations. Below we use this representation together with an EM algorithm to approximate the emission density λ.

V. A level set EM algorithm (LSEM)

In this section we shall use the level set idea to represent λ as a function that only takes a limited number of constant values. Moreover, we assume that the constant values are approximately known. Using these assumptions, we need to find the location of the discontinuities between the constant regions to identify λ. Assume that the domain Ω can be divided into a union of subregions such that all λ_b, having the same constant intensity value belong to the same subregion. For such a case, we can use level set functions to express $\lambda = \lambda(\phi)$ as in (13). Concerning the optimization problem, we utilize the fact that calculations from (8) can be carried forward by the chain rule for $\lambda(\phi)$. We let $\alpha = 0$ to neglect the TV-regularization in (8), and presently we will introduce another regularization term that is better suited in the level set framework. As the λ function is already discretized, we shall also use discretized level set functions ϕ_j, $j = 1, 2 \ldots, n$. From the chain rule we get

$$\frac{\partial L}{\partial \phi_j} = \frac{\partial L}{\partial \lambda} \frac{\partial \lambda}{\partial \phi_j}.$$

The calculation of $\frac{\partial L}{\partial \lambda}$ is given in (8) with $\alpha = 0$. We only need to have $\frac{\partial \lambda}{\partial \phi_j}$ in order to get $\frac{\partial L}{\partial \phi_j}$. If λ only takes two constant values c_1 and c_2 as in (10), it is easy to see that

$$\frac{\partial \lambda}{\partial \phi} = (c_1 - c_2)\delta(\phi),$$

where the Delta function $\delta(\phi) = H'(\phi)$. In case that we need two level set functions ϕ_1 and ϕ_2, it follows from (12) that

$$\begin{aligned}\frac{\partial \lambda}{\partial \phi_1} =&\big((c_1 - c_2 - c_3 + c_4)H(\phi_2) + c_2 - c_4\big)\delta(\phi_1), \quad \text{and}\\ \frac{\partial \lambda}{\partial \phi_2} =&\big((c_1 - c_2 - c_3 + c_4)H(\phi_1) + c_3 - c_4\big)\delta(\phi_2).\end{aligned} \tag{14}$$

For the OSL algorithm given in Section III, the total variation of λ is used as the regularization term. If we use the level set method and assume that the constant values c_i are (approximately) known, it is better to use the length of the zero level set curves as the regularization term (c.f.[21], [26]). In fact, the length of the zero level set curve for ϕ_j is

$$R(\phi_j) = \int_\Omega |\nabla H(\phi_j)|dx = \int_\Omega \delta(\phi_j)|\nabla \phi_j|dx.$$

Moreover, its derivative with respect to ϕ_j is (c.f.[26, sec.3]).

$$\frac{\partial R}{\partial \phi_j} = -\nabla \cdot \Big(\frac{\nabla \phi_j}{|\nabla \phi_j|}\Big)\delta(\phi_j).$$

In our simulations, we have used the length term as the regularization term.

Once the gradient $\frac{\partial L}{\partial \phi_j}$ is available, we can use the following gradient method (Algorithm 1 below) to find a minimizer for the optimization problem assuming that the constant values c_i are approximately known.

Algorithm 1: (Level Set EM algorithm)

- Choose initial values for ϕ_j^0 and the time step sizes Δt_j^0.
- For all the level set functions ϕ_j, update the functions as

$$\phi_j^{n+1} = \phi_j^n - \Delta t_j^n \frac{\partial L}{\partial \phi_j}(\phi_j^n).$$

- Reinitialize the level set functions ϕ_j if a "sufficient" amount of pixel values of ϕ_j have changed sign. Otherwise, go to the next iteration.

Some remarks about the implementation of the algorithm is given in the following:

- All intensity values are assumed to be approximately known.
- β weight the influence of the regularization term. An oscillatory curve may occur if β is too small and β too large will deny a proper evolution of the curve. By trial and error $\beta \in (10^{-3}, 10^{-4})$ was found to be a proper choice.

- Approximate the Delta function with $\epsilon \in (0,1)$ and use the exact Heaviside function

$$\delta_\epsilon(\phi_j) = \frac{\epsilon}{\pi(\phi_j^2 + \epsilon^2)} \qquad \text{and} \qquad H(\phi_j) = \begin{cases} 1 & \text{if } \phi_j > 0 \\ 0 & \text{if } \phi_j \leq 0. \end{cases}$$

- There are efficient numerical methods to reinitialize the level set functions. See [15], [17], [29] for details about the reinitialization of the level set functions. The numerical method we have used for the reinitialization is as in [27], [29], and we reinitialize the level set functions each 100 iteration.

VI. Numerical results

In this section we report some numerical results. The One-Step-Late (OSL) algorithm [9] is implemented and will act as a guide for results achieved by our LSEM algorithm. Below we challenge both the OSL algorithm and our LSEM algorithm with observation vectors that are corrupted with noise according to the formula: $scn_n(x) = scn_t(x) + \eta(x)\sqrt{\tau \cdot scn_t(x)}$, where $\eta(x) \in [0,1]$ are random numbers, τ direct the noise level and $scn_t(x)$ and $scn_n(x)$ are the true and noisy observation vector respectively. The relative error between the true and the noisy observation vector is measured by

$$err = \frac{\left(\int_\Omega (scn_t - scn_n)^2 dx \right)^{\frac{1}{2}}}{\left(\int_\Omega scn_t^2 \, dx \right)^{\frac{1}{2}}}.$$

One drawback with the LSEM algorithm is that all coefficients c_i in (13) have to be approximately known a priori. For some of the tests below we perturbate all coefficients c_i up to $\pm$ 10 % of their true values to see how this influence the result. In practical application such approximately information of the c_i values (tissue and isotope dependent) are normally available.

In our first example we try to reconstruct a 32×32 image of two circles, one inside the other, as seen in Fig. 5(c). Total 1536 (32 position and 48 angular views) observations with err ≈ 0.08 was given to us. Already after a few iterations with the OSL algorithm it is possible to see some distinctive mark in the PET image depicted in Fig. 2.

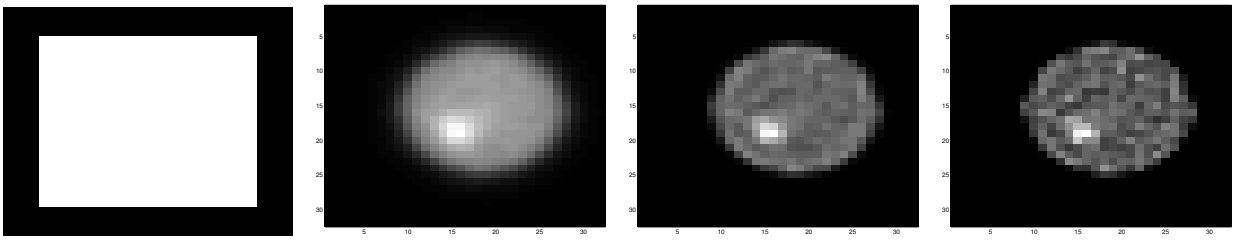

(a) Initial image (b) 5 iterations (c) 30 iterations (d) 100 iterations

Fig. 2. Evolution of a two circles using the OSL algorithm.

Two major drawbacks with the OSL algorithm are lack of termination criteria and the introduction of noise as the number of iterations increases. In Fig. 2(b) the intensity value in the outer circle is almost constant (as it should be in this test), but it is difficult to decide the exact boundary for the inner circle. After 30 iterations the edges are emphasized but so is the noise, as seen in Fig. 2(c). We must terminate the algorithm after 100 iterations, otherwise the noise will be too dominant. The same noisy observation vector was thereafter used as observation data for the LSEM algorithm and the results are given in Fig. 3. For the two level set functions, no special assumptions were made, but it is desirable to start with oscillating functions, as indicated in Fig. 3(a) and Fig. 4(a).

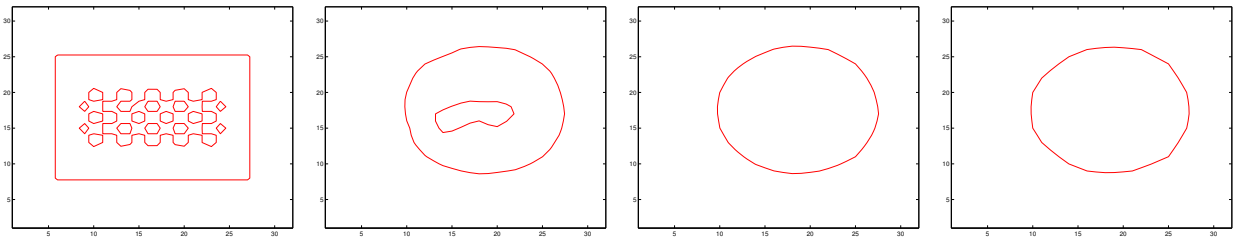

(a) Initial ϕ_1 (b) 50 iterations (c) 150 iterations (d) 650 iterations

Fig. 3. Interfaces given by the zero level set of the function ϕ_1.

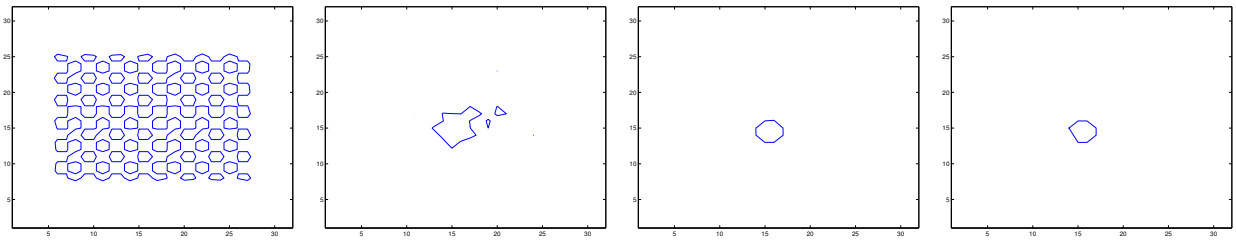

(a) Initial ϕ_2 (b) 50 iterations (c) 150 iterations (d) 650 iterations

Fig. 4. Interfaces given by the zero level set of the function ϕ_2.

In less than 200 iterations both level set functions have converged to a constant shape and these level set functions together with (12) were used to get Fig. 5(b). In this specific test we used intensity values: c_4 (dark), c_2 (gray) and $c_1 = c_3$ (light), all perturbated by $\pm$ 10 % of their true values and kept fixed during the iterations. With two level set functions we see from (11) that it is possible to identify up to 4 distinct regions. The true PET image depicted in Fig. 5(c) consists of only 3 distinct regions: background, outer circle and inner circle. To handle this, we put $c_1 = c_3$ such that 2 regions yield the same contribution to the constructed PET image.

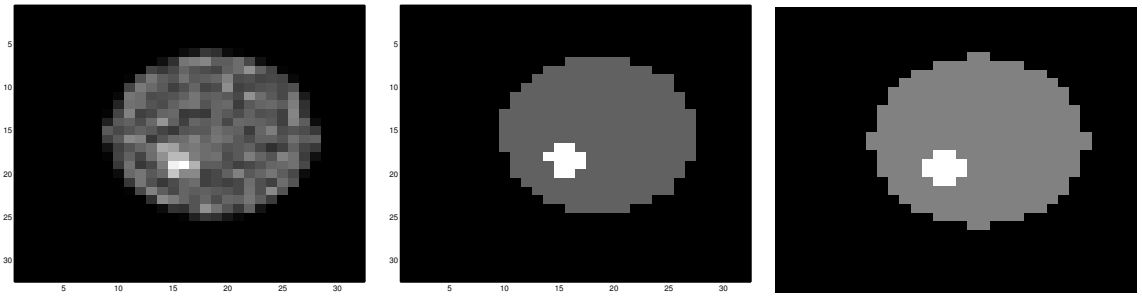

(a) OSL algorithm (b) LSEM algorithm (c) True image

Fig. 5. PET image of two circles constructed with different algorithms. A perturbation $\pm$ 10% of the true coefficients c_i are used for LSEM.

Even if this is a simple test that involves a non-medical image, it illustrates the potential in the LSEM algorithm. Sharp edges are implicit given for the PET image and different regions do not suffer from inhomogeneities caused by noise. Moreover, the geometry of the objects in Fig. 5(b) are given by the level set functions in Fig. 3(d) and Fig. 4(d).

Notice the differences in the shape of the inner circle revealed by the two algorithms in Fig. 5. Unfortunately the outer circle in Fig. 5(b) seems smaller than the outer circle in Fig. 5(c) and is holding another gray scale value. Remember that each coefficient c_i are linked to a unique region $\Omega_i \subseteq \Omega$. Since these coefficients are perturbated and kept fixed in this test, the regions Ω_i, $i = 1, 2, 3, 4$, must compensate to fit the observation vector. The two circles where reconstructed perfectly when the true c_i values were used.

In our next example the interior structure of the PET image is more complicated. We try to reconstruct a 32×32 image of the brain from 1536 observations (32 position and 48 angular views). In Fig. 6 the results obtained with the OSL algorithm are given.

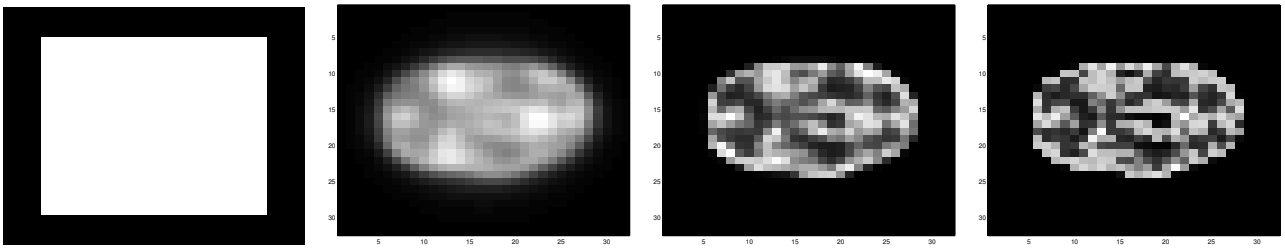

(a) Initial image (b) 5 iterations (c) 100 iterations (d) 1000 iterations

Fig. 6. Evolution of a brain image with the OSL algorithm.

In this test, we use the true observation vector without adding noise to it. Even so, only few pixels are approximated to the correct intensity value by the OSL algorithm. Due to this, important anatomical or functional details may be lost. We also used the true observation vector as observation data to the LSEM algorithm. An evolution of the two functions ϕ_1 and ϕ_2 are given in Fig. 7 and Fig. 8 respectively.

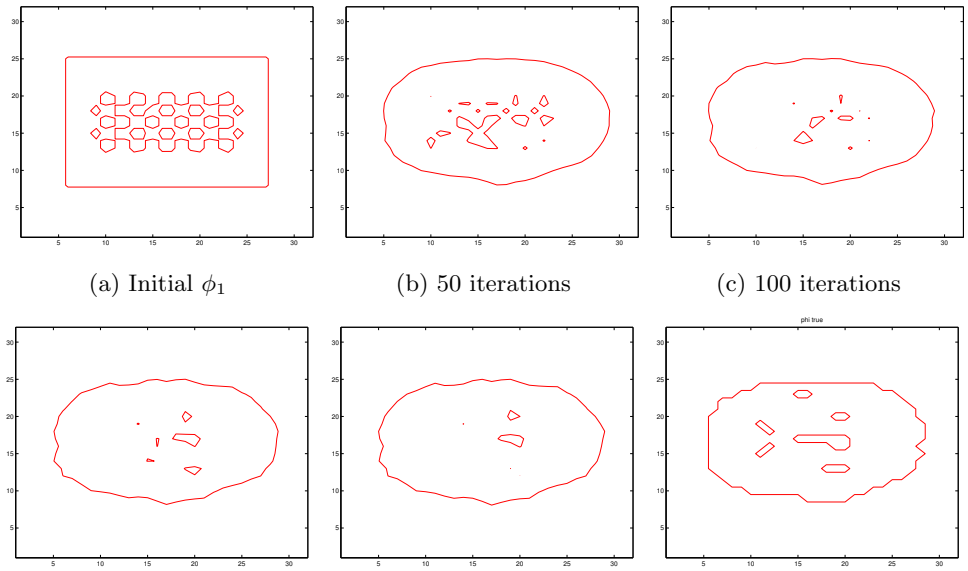

(a) Initial ϕ_1 (b) 50 iterations (c) 100 iterations

(d) 500 iterations (e) 2000 iterations (f) True ϕ_1

Fig. 7. Interfaces given by the zero level set of the function ϕ_1.

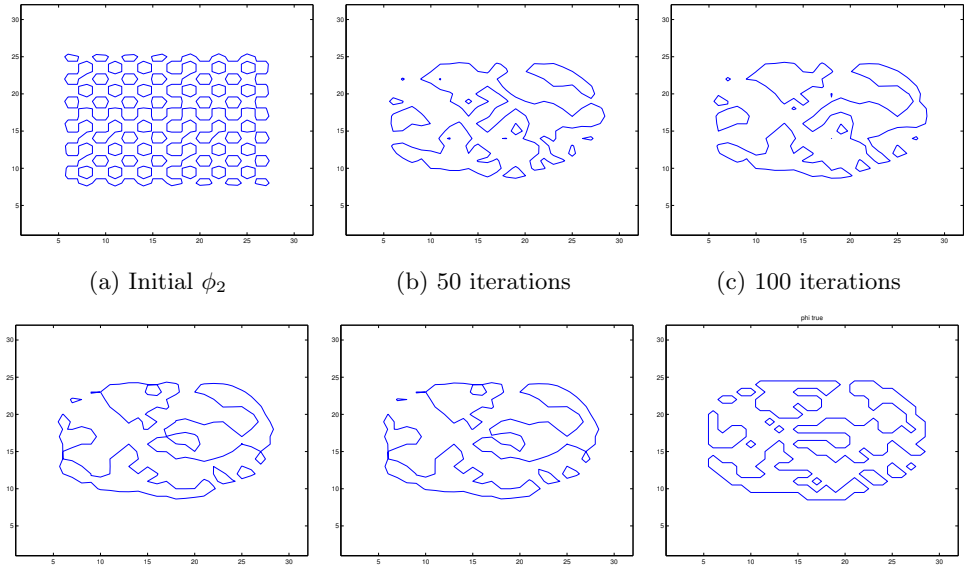

(a) Initial ϕ_2 (b) 50 iterations (c) 100 iterations

(d) 500 iterations (e) 2000 iterations (f) True ϕ_2

Fig. 8. Interfaces given by the zero level set of the function ϕ_2.

In less than 2000 iterations the two level set functions have converged. Combining ϕ_1 from Fig. 7(e) and ϕ_2 from Fig. 8(e) together with (12) we get the PET image depicted

in Fig. 9(b). In this test we used: c_4 (background), c_2 (gray matter) and $c_1 = c_3$ (white matter).

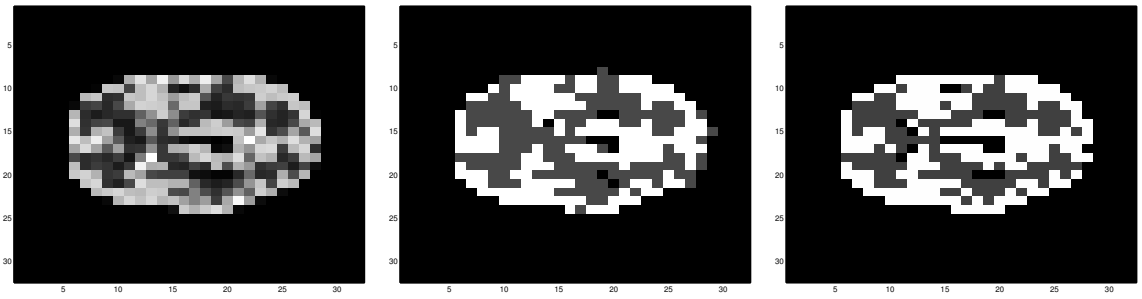

(a) OSL algorithm (b) LSEM algorithm (c) True image

Fig. 9. Construction of a PET image with different algorithms. The true observation vector was given, and for the LSEM algorithm a perturbation $\pm 10\%$ of the true intensity values was used.

In Fig. 9(a) we observe a specter of intensity values inside regions that should take a constant value. Further, there are unsharp boundaries between the tissue classes. By construction, only 3 intensity values occur in the PET image were found by the LSEM algorithm. This is a strength compared with the PET image constructed by the OSL algorithm. One can use some kind of threshold technique to separate the intensity values in Fig. 9(a) into 3 classes, but we did not find this approach to produce any better result than the LSEM algorithm. Neither the LSEM algorithm is able to recover all the fine details in the PET image, particularly some part of the dark region are mixed up with gray region inside the brain in Fig. 9(b).

In our final examples we challenge our algorithm with a 64×64 segmented MRI slice of the brain. We used the true intensity values: c_4 (background), c_2 (gray matter) and $c_1 = c_3$ (white matter) and 6144 (64 position and 96 angular views) observations. Compared with Fig. 5(c) and Fig. 9(c) the inner structure to be recovered here are more complicated, as seen in Fig. 12(c). An evaluation of the ϕ_1 and ϕ_2 functions are given Figs. 10-11.

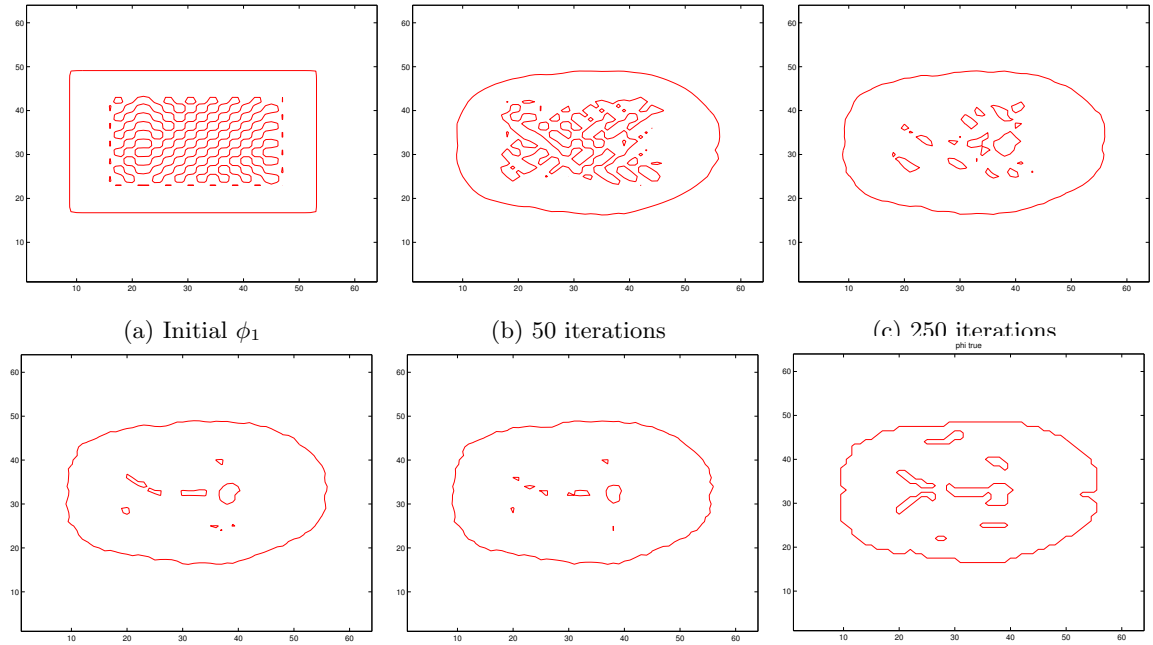

(a) Initial ϕ_1 (b) 50 iterations (c) 250 iterations

(d) 1000 iterations (e) 2800 iterations (f) True ϕ_1

Fig. 10. Interfaces given by the zero level set of ϕ_1 for a brain image with a finer resolution (64×64).

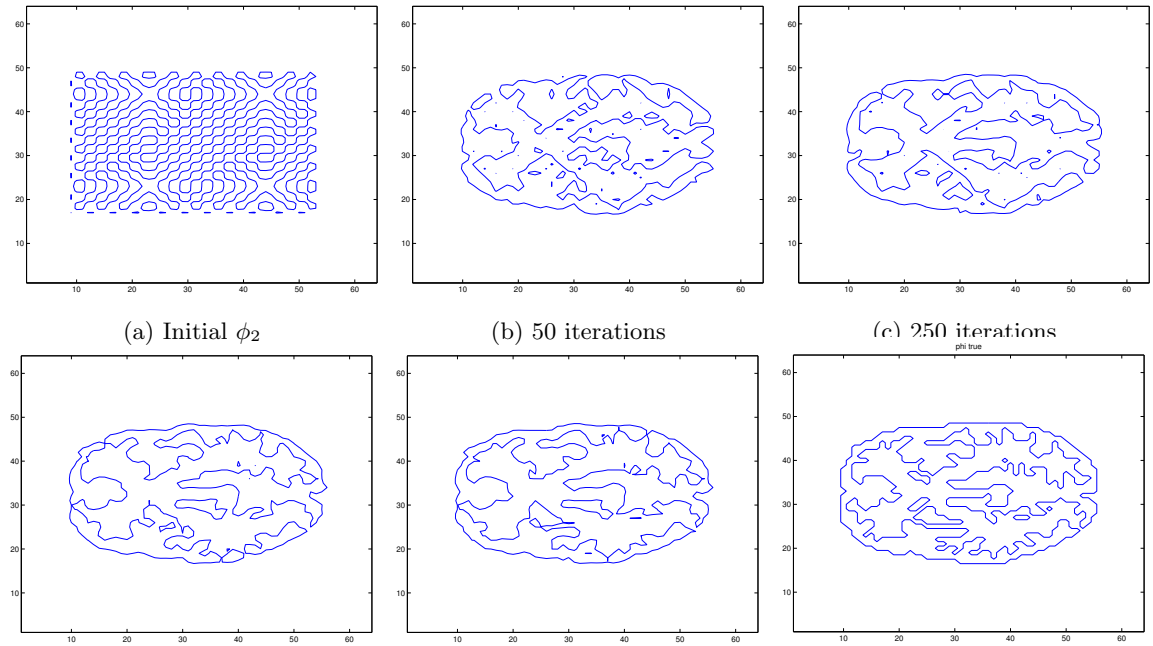

(a) Initial ϕ_2 (b) 50 iterations (c) 250 iterations

(d) 1000 iterations (e) 2800 iterations (f) True ϕ_2

Fig. 11. Interfaces given by the zero level set of ϕ_2 for a brain image with a finer resolution (64×64).

In less than 250 iterations we have a good approximation for the shape of the two level set functions. At convergence, almost all important information for ϕ_2 is recovered. The interior structure for ϕ_1 is not that nicely recovered. This will influence the appearance of the PET image, as seen in Fig. 12(b).

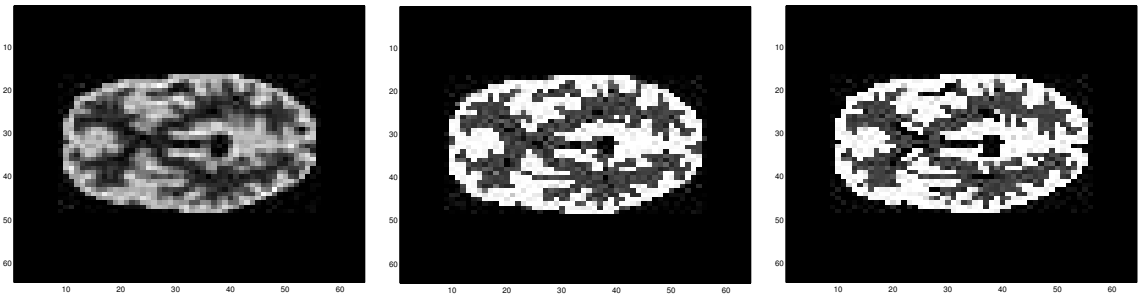

(a) OSL algorithm (b) LSEM algorithm (c) True image

Fig. 12. 64×64 segmented MRI slice of the brain.

Also in this test it seems that LSEM algorithm mixed up some part of the dark region with the gray region inside the brain. The reason for this may be that $\frac{1}{4}c_2{=}c_3{=}c_1$, meaning that 4 misplaced pixels with intensity value c_2 generate the same error as one misplaced pixel with intensity value c_1 or c_3. Even so, due to the similarity between Fig. 12(b) and Fig. 12(c), we see that the LSEM algorithm produce better result than what we can achieve with the OSL algorithm in Fig. 12(a).

To obtain improved reconstructions one approach is to use priors that reflect the nature of the underlying radio-nuclide distribution. Recently there has been considerable interest in incorporating side information derived from highly correlated anatomical information (such as MR) in the form of Bayesian priors [30], [31]. The main attraction of this approach is that one can expect to obtain improved reconstructions to the extent that functions follows anatomy.

Assume that MR or SPECT observations are used to generate information of the PET image, partly or in the entire domain Ω. Below we will demonstrate that such information will improve the image construction capacity noticeable. First, we assume both ϕ_1 and ϕ_2 to be known in the left quarter of Ω. The initial state for both phases and the PET image are depicted in the first row of Fig. 13, and the final solutions are given in the second row.

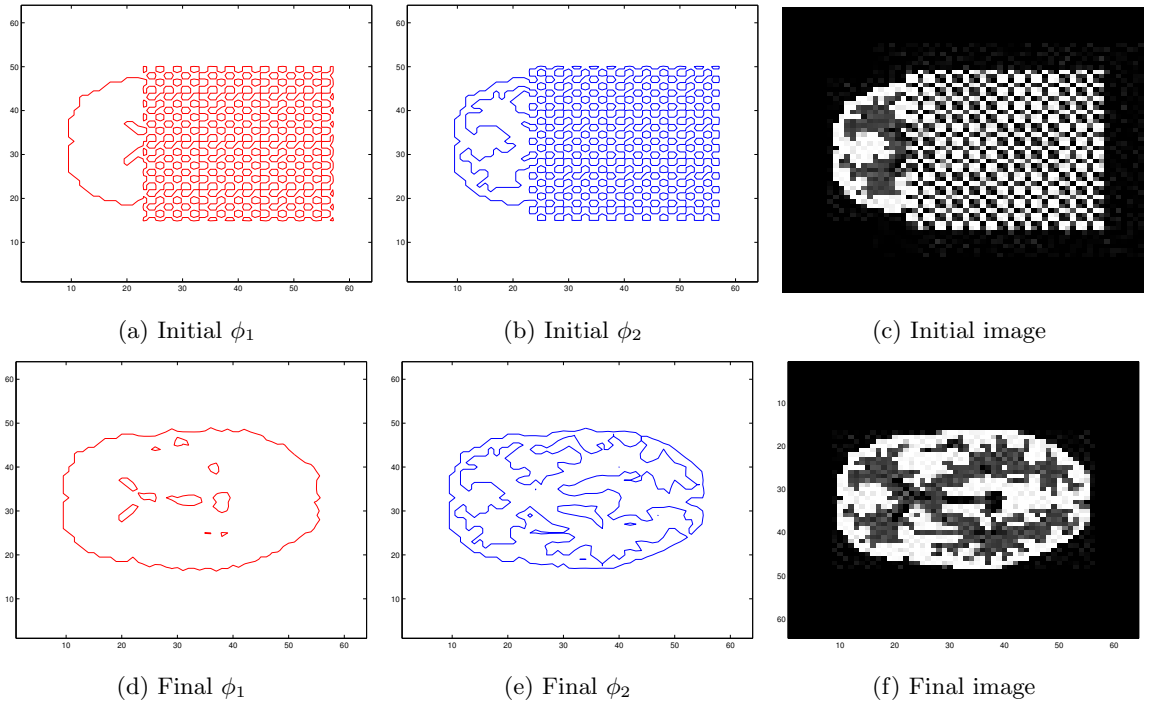

(a) Initial ϕ_1 (b) Initial ϕ_2 (c) Initial image

(d) Final ϕ_1 (e) Final ϕ_2 (f) Final image

Fig. 13. Reconstruction of a 64×64 brain image assuming that the level set functions are known in the left quarter of the domain.

Compared with the results in Fig. 12 we see that a priori information of the geometrical objects improves the reconstruction. Next, we assume both ϕ_1 and ϕ_2 to be known in the left half of Ω. The initial state for both phases and the PET image are depicted in the first row of Fig. 14, and the final solutions are given in the second row.

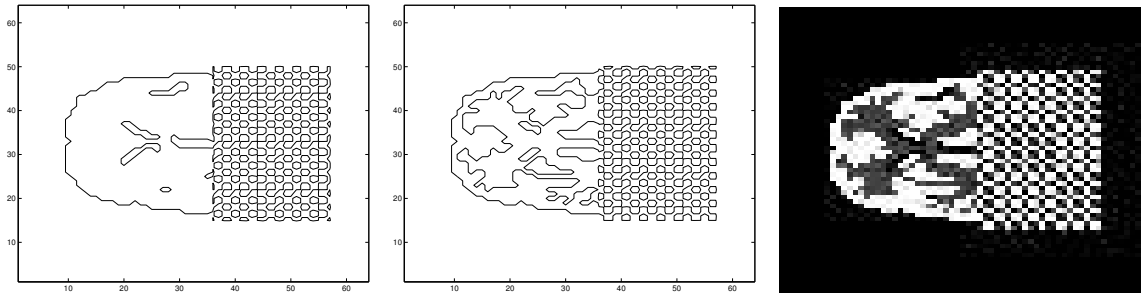

(a) Initial ϕ_1 (b) Initial ϕ_2 (c) Initial image

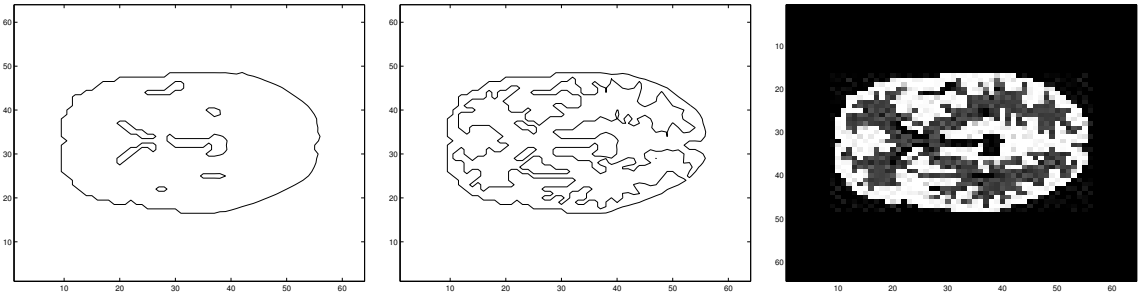

(d) Final ϕ_1 (e) Final ϕ_2 (f) Final image

Fig. 14. Reconstruction of a 64×64 brain image assuming that the level set functions are known in the left half of the domain.

We only visualize ϕ_1 and ϕ_2 at their steady state where a perfect construction of the PET image is achieved.

Another situation is that one phase can be fixed to a constant shape due to external measurements while the other phase evolves freely. Below we fix ϕ_1 to its true shape as in Fig. 10(f), and let ϕ_2 evolve from its initial state as given in Fig. 15.

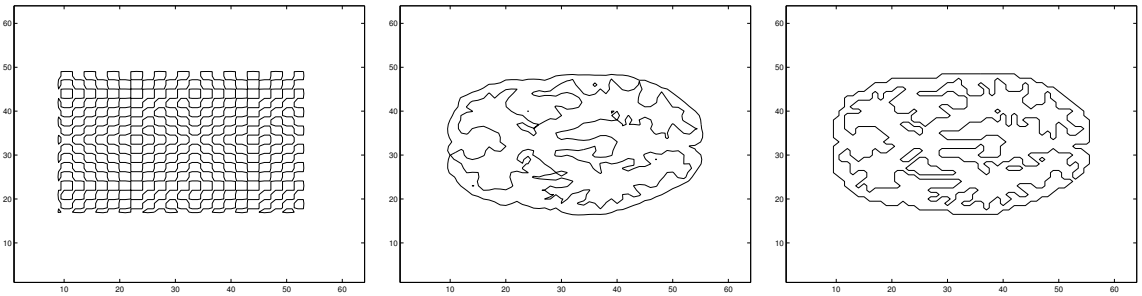

(a) Initial ϕ_2 (b) Final ϕ_2 (c) True image

Fig. 15. Evaluation of ϕ_2 if ϕ_1 known

Again, a perfect result was achieved at steady state. The same occurs if we fix ϕ_2 to its true shape and let ϕ_1 evolve. A perturbation of the c_i values up to $\pm 10\%$ was used in both tests.

Acknowledgments

The authors would like to thank Sung-Cheng Huang at the Department of Molecular and Medical Pharmacology, University of Los Angeles, for providing the PET data for all the numerical examples in this paper.

References

[1] S. R. Deans, *The Radon Transform and some of its Applications*, Wiley, New York, 1983.

[2] M. Bertero and P. Boccacci, *Introduction to Inverse Problems in Imaging*, Bristol: Institute of Physics Publishing, 1998.

[3] M. Bertero and E.R. Pike, *Parametric reconstruction of a biomagnetic imaging. (eds.) Inverse Problems in Scattering and Imaging (p. 156-163)*, Adam Hilger, Bristol, 1992.

[4] A. P. Dempster, N. M. Laird, and D. M. Rubin, "Maximum likelihood for incomplete data via the EM algorithm," *J. Roy. Stat. Soc.*, vol. Ser. B, no. 39, pp. 1–38, 1977.

[5] K. Lange and R. Carson, "EM reconstruction algorithms for emission and transmission tomography," *Journal of Computer Assisted Tomography*, vol. 8, no. 2, pp. 306–316, 1984.

[6] L. A. Sheep and Y. Vardi, "Maximum likelihood reconstruction for emission tomography," *IEEE Transactions on Medical Imaging*, vol. MI-1, no. 2, pp. 113–122, 1982.

[7] E. Veklerov and J. Llacer, "Stopping rule for the MLE algorithm based on statistical hypothesis testing," *IEEE Transaction on Medical Imaging*, vol. MI-8, pp. 313–319, 1987.

[8] T. Hebert and R. Leahy, "A generalized EM algorithm for 3-D Bayesian reconstruction from Poisson data using Gibbs priors," *IEEE Transaction on Medical Imaging*, vol. MI-8, pp. 194–202, 1989.

[9] P. Green, "Bayesian reconstruction form emission tomography using a modified EM algorithm," *IEEE Transaction on Medical Imaging*, vol. MI-9, pp. 84–93, 1990.

[10] S. Alenius and U. Ruotsalainen, "Bayesian image reconstruction for emission tomography based on median root prior," *European Journal of Nuclear Medicine*, vol. 24, no. 3, pp. 258–265, 1997.

[11] L.I. Rudin, S. Osher, and E. Fatemi, "Nonlinear total variation based noise removal algorithms," *Physica D*, vol. 60, pp. 259–268, 1992.

[12] M. Lysaker, S. Osher, and X.-C. Tai, "Noise Removal Using Smoothed Normals and Surface Fitting," *IEEE Tran. Image Processing*, To appear in 2004.

[13] E. Jonsson, S. C. Huang, and T. Chan, "Total variation regularization in positron emission tomography," Tech. Rep., CAM Report 98-48, UCLA, Math. Depart., 1998.

[14] S. Osher and J. A. Sethian, "Fronts propagating with curvature dependent speed," *J. Comput. Phys.*, , no. 79, pp. 12–49, 1988.

[15] S. Osher and R. Fedkiw, "Level set methods: An overview and some recent results," *J. Comput. Phys.*, vol. 169, no. 2, pp. 463–502, 2001.

[16] J. A. Sethian, *Level set methods and fast marching methods*, vol. 3 of *Cambridge Monographs on Applied and Computational Mathematics*, Cambridge University Press, Cambridge, second edition, 1999, Evolving interfaces in computational geometry, fluid mechanics, computer vision, and materials science.

[17] S. Osher and R. Fedkiw, *Level set methods and dynamic implicit surfaces*, vol. 153 of *Applied Mathematical Sciences*, Springer-Verlag, New York, 2003.

[18] O. Dorn, E. L. Miller, and C. M. Rappaport, "A shape reconstruction method for electromagnetic tomography using adjoint fields and level sets," *Inv. Probl*, vol. 16, no. 5, pp. 119–1156, Oct 2000.

[19] D. F. Yu and J. A. Fessler, "Edge-Preserving Tomographic Reconstruction with Nonlocal Regularization," *IEEE Trans. Med. Imaging*, vol. 21, no. 2, pp. 159–173, 2002.

[20] H. Feng, W. C. Karl, and D. A. Castañon, "A Curve Evolution Approach to Object-Based Tomograpic Reconstruction," *IEEE Trans. Image Proc*, vol. 12, no. 1, pp. 44–57, 2003.

[21] L. A. Vese and T. F. Chan, "A new multiphase level set framework for image segmentation via the Mumford and Shah model," *International Journal of Computer Vision*, vol. 50, pp. 271–293, 2002.

[22] J. Llacer, S. Andreae, E. Veklerov, and E. J. Hoffman, "Towards a practical implementation of the MLE algorithm for positron emission tomography," *IEEE Trans. Nucl. Sci.*, vol. 33, no. 1, pp. 468–477, 1986.

[23] E. Veklerov, J. Llacer, and E. J. Hoffman, "MLE Reconstructions of a Brain Phantom Using a Monte Carlo Transition Matrix and a Statistical Stopping Rule," *IEEE Trans. Nucl. Sci.*, vol. 35, no. 1, pp. 603–607, 1988.

[24] D. L. Snyder and M. I. Miller, "The use of sieves to stabilize images produced with EM algorithm for emission tomography," *IEEE Trans. Nucl. Sci.*, vol. NS-32, pp. 3864–3872, 1985.

[25] J. Lie, M. Lysaker, and X.-C. Tai, "A Variant of the Level Set Method and Applications to Image Segmentation," Tech. Rep., CAM Report 03-50, UCLA, Math. Depart., 2003.

[26] X.-C. Tai and T. F. Chan, "A Survey on Multiple Set Methods With Applications for Identifying Piecewise Constant Function," *International J. Numer. Anal. Modelling*, vol. 1, pp. 157–172, 2004, Available online at http://www.mi.uib.no/%7Etai/.

[27] T. F. Chan and X.-C. Tai, "Level set and total variation regularization for elliptic inverse problems with discontinuous coefficients," *Journal of Computational Physics*, vol. 193, pp. 40–66, 2003.

[28] T. F. Chan and L. A. Vese, "Image segmentation using level sets and the piecewise constant Mumford-Shah model," Tech. Rep., CAM Report 00-14, UCLA, Math. Depart., April 2000, revised December 2000.

[29] D. Peng, B. Merriman, S. Osher, H. Zhao, and M. Kang, "A PDE-based fast local level set method," *J. Comput. Phys.*, vol. 155, no. 2, pp. 410–438, 1999.

[30] B. A. Ardakani, M. Braun, B. F. Hutton, I. Kanno, and H. Ida, "Minimum cross-entropy reconstruction of PET images using prior anatomical information," *Phys. Med. Biol.*, vol. 41, no. 11, pp. 2497–2517, 1996.

[31] G. Gindi, M. Lee, A. Rangarajan, and I. G. Zubal, "Bayesian reconstruction of functional images using anatomical as priors," *IEEE Trans. Med. Imaging*, vol. 12, no. 4, pp. 673–680, 1993.